


Article

Equilibrium, Kinetics and Thermodynamics of Chromium (VI) Adsorption on Inert Biomasses of *Dioscorea rotundata* and *Elaeis guineensis*

Angel Villabona-Ortíz ¹, Ángel González-Delgado ² and Candelaria Tejada-Tovar ^{1,*}

¹ Process Design and Biomass Utilization Research Group (IDAB), Chemical Engineering Department, Universidad de Cartagena, Avenida del Consulado St. 30, Cartagena de Indias 130015, Colombia; avillabona@unicartagena.edu.co

² Nanomaterials and Computer Aided Process Engineering Research Group (NIPAC), Chemical Engineering Department, Universidad de Cartagena, Avenida del Consulado St. 30, Cartagena de Indias 130015, Colombia; agonzalezd1@unicartagena.edu.co

* Correspondence: ctejadat@unicartagena.edu.co

Abstract: Adsorption equilibrium and kinetics on lignocellulosic base adsorbents from oil palm bagasse (OPB) and yam peels (YP) were studied for the removal of hexavalent chromium present in aqueous solution, in a batch system, evaluating the effect of temperature, adsorbent dose and particle size on the process. Isotherms were fitted to Langmuir, Freundlich and Dubinin–Radushkevich isothermal models. Kinetic data were adjusted to the pseudo-first-order, pseudo-second-order and Elovich models. Thermodynamic parameters were estimated by the van't Hoff method. From characterization of adsorbents, the presence of a porous surface typical of lignocellulosic materials was found, with hydroxyl, amine and carboxyl functional groups. It was also found that the highest adsorption capacity was obtained at 0.03 g of adsorbent, 55 °C and 0.5 mm, reporting an adsorption capacity of 325.88 and 159 mg/g using OPB and YP, respectively. The equilibrium of adsorption on OPB is described by Langmuir and Freundlich isotherms, while that of YP is described by Dubinin–Radushkevich's model, indicating that the adsorption is given by the ion exchange between the active centers and the metallic ions. A maximum adsorption capacity was obtained of 63.83 mg/g with OPB and 59.16 mg/g using YP, according to the Langmuir model. A kinetic study demonstrated that equilibrium time was 200 min for both materials; kinetic data were described by pseudo-second-order and Elovich models, thus the mechanism of Cr (VI) adsorption onto the evaluated materials is dominated by a chemical reaction. The thermodynamic study determined that the elimination of YP is endothermic, irreversible and not spontaneous, while for OPB it is exothermic, spontaneous at low temperatures and irreversible.



Citation: Villabona-Ortíz, A.; González-Delgado, Á.; Tejada-Tovar, C. Equilibrium, Kinetics and Thermodynamics of Chromium (VI) Adsorption on Inert Biomasses of *Dioscorea rotundata* and *Elaeis guineensis*. *Water* **2022**, *14*, 844. <https://doi.org/10.3390/w14060844>

Academic Editors: Cristina Palet and Julio Bastos-Arrieta

Received: 12 January 2022

Accepted: 3 March 2022

Published: 8 March 2022

Publisher's Note: MDPI stays neutral with regard to jurisdictional claims in published maps and institutional affiliations.



Copyright: © 2022 by the authors. Licensee MDPI, Basel, Switzerland. This article is an open access article distributed under the terms and conditions of the Creative Commons Attribution (CC BY) license (<https://creativecommons.org/licenses/by/4.0/>).

Keywords: bio-adsorption; Langmuir; Freundlich; Dubinin–Radushkevich

1. Introduction

The presence of heavy metal ions in wastewater is a serious problem due to the discharge of contaminated effluents into the environment [1]. Among the pollutants generally discharged to water bodies are heavy metals; these are found in the wastewater from industrial processes involving inks, metallurgy, batteries, oil, mining and tanneries, among others [2]. Chromium appears in aqueous systems in the forms +3 and +6, with the hexavalent chromium being much more toxic than the trivalent [3]; these ions are widely used in the manufacture of inks, industrial dyes and paint pigments, chrome plating, aluminum anodizing and other cleaning, coating and electroplating operations of metals and gold mining, among others [4].

Several removal methods have been used in the capture of hexavalent chromium due to its toxic health effects [5]. These technologies include filtration, chemical precipitation,

adsorption, electrodeposition and membrane systems or even ion exchange processes [6]. Among these methods, bio-adsorption is one of the most economically favorable methods; it is technically easier, with high availability of adsorbents and the possibility of reuse [7]. The removal of hexavalent chromium has been studied using biomasses from different origin, such as corn residues [8], coffee pulp [3], kenaf [9], oil palm ash [5] and peels of lime [4], nut [10], orange [11] and plantain [12], obtaining good performance of biomaterials due to the presence of hydroxyl, carboxyl, amino and carbonyl functional groups, due to their lignocellulosic nature [13].

In Colombia, the intensive and extensive planting of African palm for use in oil extraction generates large volumes of waste during the process, including palm bagasse and shells; due to the 60% of increase in oil production from oil palm, about 500,000 tons of waste are generated per year [14]. Although the shell obtained as a by-product is generally used as fuel for boilers and composting, the residual fiber is a rejected product that does not have a use after fruit separation. Thus, the recovery of waste such as waste fiber is very important to mitigate its effects on the environment, and guarantee a sustainable process. Among the various potential applications that could be given to residual palm fiber, its use as an adsorbent in the treatment of water contaminated with heavy metals, among a wide range of applications, seems attractive taking into account the reported removal yields for similar residues [15]. In addition, Colombia was ranked among the 12 countries with the highest yam production worldwide and ranked first in terms of product yield with 28.3 tons per planted hectare, generating after harvesting around 5000 tons of waste per year [16].

In the studies of hexavalent chromium adsorption, several variables have been evaluated such as adsorbent dose, initial concentration, particle size and temperature, which are parameters that affect the availability of active sites of the adsorbent, the diffusive and mass transfer phenomena of the pollutant from the solution to the adsorbent, the exposed surface area and the mechanisms that dominate the adsorption of the pollutant [17]. In this sense, the determination of the adsorption isotherm and thermodynamic parameters (change in Gibbs free energy, enthalpy, and entropy) are necessary for helping to understand the mechanisms and phases involved in chromium adsorption [18]. Thus, the objective of this study was to determine the effect of adsorbent dose, particle size and temperature on the adsorption capacity of chromium (VI) using yam peels (YPs) and oil palm residues (OPBs) in a batch system. Adsorption equilibrium on adsorbents was studied and fitted to Langmuir, Freundlich, and Dubinin–Radushkevich isothermal models. Thermodynamic parameters were estimated by the van't Hoff graphical method.

2. Methodology

2.1. Materials and Reagents

Oil palm waste (OPB) was obtained as a rejection product of the oil extraction process and yam peels as a by-product of post-harvest handling in the department of Bolívar (Colombia). The lignocellulosic material was washed, sun-dried to a constant mass, and subjected to size reduction in a roller mill and size classification in a sieve-type shaker on stainless steel meshes. The 100 mg/L chromium solution used in the adsorption tests was prepared with analytical grade potassium dichromate ($K_2Cr_2O_7$) (Merck Millipore[®], Burlington, MA, USA). To adjust the pH we used hydrochloric acid (HCl) and sodium hydroxide (NaOH) 0.5 M solutions to adjust to pH 2 [8]. All the reagents used in the present study were analytical grade.

The adsorbents were characterized by Fourier transform infrared spectroscopy analysis in a Shimadzu (Kyoto, Japan) IRAinfinity-1S spectrophotometer model, with a frequency of 32 scans between 400 and 4000 cm^{-1} , for the purpose of identifying the functional groups that would work as active centers during the process of metal removal. The morphological properties and elemental composition of the biomass were determined using a scanning electron microscope together with an energy dispersive spectroscopy (SEM-EDS) model

JSM-6490LV JEOL Ltd. (JEOL Ltd., Akishima, Japan). All trials were conducted before and after the metal removal process.

2.2. Adsorption Tests

The YH and OPB wastes were washed, sun-dried to remove moisture and reduced in size in a hand-roller mill, and sized in a vibrating sieve machine using stainless steel meshes. The materials were stored in airtight plastic bags to keep them in good condition.

For the experimental development, a continuous factor central composite design with a star-type response surface was selected and is shown in Table 1, the design was made using the software Statgraphics Centurion XVI.II. For the classification of biomaterial sizes, mesh numbers 120, 45, 35, 18 and 16 were used, which select size ranges of 0.1060.125 mm, 0.3–0.355 mm, 0.425–0.5 mm, 1.0–1.18 mm and 1.18–1.4 mm, respectively.

Table 1. Experimental design.

Independent Variables	Units	Range and Levels				
		Lower Level	Low Level	Center Point	High Level	Higher Level
Particle size	mm	0.14	0.355	0.5	1.0	1.22
Adsorbent dose	g	0.003	0.15	0.325	0.5	0.62
Temperature	°C	29.8	40	55	40	80

Adsorption experiments were performed in a batch system using an orbital shaker by contacting 100 mL of solution at pH 2 [19], for 200 rpm per 24 h, at the conditions described in Table 1. The remaining concentration of hexavalent chromium in the solution was determined by ASTM D 1687-02, by adding 48 mL of deionized water, 2 mL of 1,5-diphenylcarbazide solved in acetone and 0.5 mL of Cr (VI) sample in acid conditions; for this purpose, a Biobase spectrophotometer BK-UV1900 was used, setting the wavelength to 540 nm [20]. The spent adsorbent after adsorption tests was removed by filtration, using cellulose membrane microfilters of 0.45 µm. The adsorption capacity was determined according to Equation (1), where q_t (mg/g) is the adsorption capacity of the material, C_0 and C_f (mg/L) are the initial and final concentration of chromium, V (L) is the volume of solution and m (g) is the mass of adsorbent. In order to evaluate the reproducibility of the results, the experiments were conducted in triplicate.

$$q_t = \frac{(C_0 - C_f) * V}{m} \quad (1)$$

2.3. Adsorption Equilibrium

An adsorption isotherm describes the equilibrium of the material's adsorption on a surface at a constant temperature; it represents the amount of material bound to the surface as a function of the material present in the gas phase or dissolution, as well as determining the interactions that control the process [21]. The data from the effect of concentration of the solution (25, 50, 75, 100, 125 and 150 mg/L) were adjusted to the models of Langmuir, Freundlich, and Dubinin–Radushkevich.

Freundlich's isotherm (Equation (2)) assumes the formation of multilayers during the adsorption process due to the different activation energies and affinities of the active centers of the adsorbent [22].

$$q_e = k_f C_e^{1/n} \quad (2)$$

where k_f is the Freundlich constant and represents the distribution coefficient (L/g), n represents the adsorption intensity and indicates the heterogeneity of the active sites, q_e is the amount of metal adsorbed at equilibrium (mg/g) and C_e is the residual metal concentration in solution (mg/L) [23].

Langmuir's adsorption isotherm (Equation (3)) quantitatively describes the deposition of ions uniformly on an adsorbing surface as a function of the concentration of the adsorbed material in the liquid with which it is in contact [24].

$$q_e = q_{max} \frac{K_L C_e}{1 + K_L C_e} \quad (3)$$

where q_{max} is the maximum adsorption of the Langmuir model (mg/g) and K_L is the Langmuir constant and can be correlated with the variation of the adsorption area and the porosity of the adsorbent [23].

The Dubinin–Radushkevich isothermal model (Equation (4)) is a semi-empirical equation applied to express the mechanism of adsorption with Gaussian energy distribution on heterogeneous surfaces and is only suitable for an intermediate range of adsorbate concentrations because it exhibits asymptotic behavior. It assumes a multilayer character involving Van Der Waals forces, applicable for physical adsorption processes; it is usually applied to differentiate between physical and chemical adsorption of metal ions [25].

$$q_e = q_{DR} e^{-k_{DR} \varepsilon^2} \quad (4)$$

$$\varepsilon = RT \times \ln \left(1 + \frac{1}{C_e} \right) \quad (5)$$

$$E = \frac{1}{\sqrt{2K_{DR}}} \quad (6)$$

where ε^2 is the Polanyi potential, K_{DR} is the Dubinin–Radushkevich constant related to adsorption energy (mol^2/kJ^2), E is the average adsorption energy per molecule of adsorbate required to transfer one mol of ion from solution to the adsorbent surface (kJ/mol), R is the gas constant (8.314 J/mol K) and T is the absolute temperature.

2.4. Kinetic Study

After the experimental design proposed in Table 1, the best conditions were estimated and the kinetic study was carried out, putting 10 mL of solution in contact with the adsorbent, taking 8 samples at different time intervals in 24 h. The experimental kinetics data were modeled to the pseudo-first-order, pseudo-second-order and Elovich models through non-linear adjustment in the Origin Pro 9 program, maximizing R^2 ; equations are shown in Table 2.

Table 2. Kinetic models evaluated in this work.

Kinetic Model	Equation	Parameters
Pseudo-first-order	$q_t = q_e (1 - e^{-k_1 t})$	k_1 (min^{-1}): kinetic constant of pseudo-first-order
Pseudo-second-order	$q_t = \frac{t}{\left(\frac{1}{q_e^2 k_2}\right) + \left(\frac{t}{q_e}\right)}$	k_2 (g/mg min): kinetic constant of pseudo-first-order
Elovich	$q_t = \frac{1}{\beta} \ln(\alpha\beta) + \frac{1}{\beta} \ln(t)$	β (g/mg): exponent indicating the capacity of adsorption α (mg/g min): Elovich constant indicating the rate of adsorption

2.5. Estimation of Thermodynamic Parameters

The thermodynamic parameters were estimated using the graphical method based on the Vant't Hoff equation in order to determine the spontaneity, type of adsorption and predict the magnitude of changes on the surface of the adsorbent [26]. The analysis of these parameters will make it possible to estimate the feasibility of the adsorption process and

the effect of temperature [27]. We estimated the change in Gibbs' standard free energy (ΔG^0), the standard enthalpy (ΔH^0) and standard entropy (ΔS^0). Adsorption experiments were performed by varying the temperature from 29.8 to 81 °C, considering the conditions established in the design of experiments; then, a graph of $\ln(K_c)$ vs. T^{-1} was plotted and the parameters were calculated using the following equations:

$$\ln K_c = \frac{-\Delta H^0}{RT} + \frac{\Delta S^0}{R} \quad (7)$$

$$\Delta G^0 = -RT \times \ln K_c \quad (8)$$

$$K_c = \frac{C_{ac}}{C_{se}} \quad (9)$$

where R is the constant of the ideal gases (8.314 J/mol K), K_c is the constant of equilibrium, C_{ac} is the concentration of the adsorbate in the equilibrium contained on the surface of the adsorbent, C_{se} is the concentration in solution at equilibrium and T is the absolute temperature. ΔH^0 (kJ/mol K) and ΔS^0 (kJ/mol) are determined from the slope and the intercept with the y -axis of the Arrhenius graph of $\ln K_c$ vs. T^{-1} , respectively.

The final disposition of the residues produced during the experimental part of this research was made according the institutional politics of the Universidad de Cartagena-Colombia. Liquid residue products of experimentation were collected by a specialized company hired for this purpose. Solid residues, such as saturated adsorbent, were dried and used as aggregates in mortars, in order to evaluate their lixiviation possibility in structures like concrete, asphalt and brick.

3. Results

3.1. Characterization of OPB and YP

The adsorption process is a complex phenomenon controlled by several mechanisms, which are generally sequential. Among these, the surface chemistry and the pore structure of the adsorbents have a considerable effect on the process, since they establish the transfer and diffusion interactions for the capture of the metal ions [28]. Thus, the adsorbents were characterized by Brunauer–Emmett–Teller (BET) analysis, obtaining that YP presented a surface area of 0.9463 m²/g, pore volume of 0.005452 m³/g and pore size of 23.04419 nm; while OPB presented 2.7317 m²/g, 0.011207 m³/g and 16.41 nm for surface area, volume and pore size, respectively. It was established that the OPB area is higher than the YP, which could be due to its fibrous structure since it would present higher surface wear, as it is a residue from the extraction of palm oil, leading to a change in the arrangement of cellulose, hemicellulose and lignin structures in the material structure and causing an increase in surface area [29]. Both materials have pore sizes between 2 and 50 nm, which indicates that they are mesoporous materials; this makes them suitable adsorbents for adsorption in the liquid phase, since it facilitates the diffusion of the adsorbent in the adsorbent structure [30].

Figures 1 and 2 show the scanning electron microscopy (SEM) images of the adsorbents under study. YP has an irregular and porous surface, which allows a large interface for heterogeneous biosorption, while OPB has a smooth, fibrous surface, which presents a certain porosity in its structure that is typical of lignocellulosic materials [31].

Table 3 shows the chemical composition in weight % and atomic % for the evaluated adsorbents obtained from the EDS analysis; carbon and oxygen are the ones with the highest presence in all the materials studied, which can be attributed to their organic nature [28]. For YP there is 57.07% C, 39.05% O, 1.65% K and elements in small proportions: Si, P, S, Ca, Fe and Cu. For OPB, 59.07% C, 38.85% O, 1.92% Si, Ca and Cu were obtained.

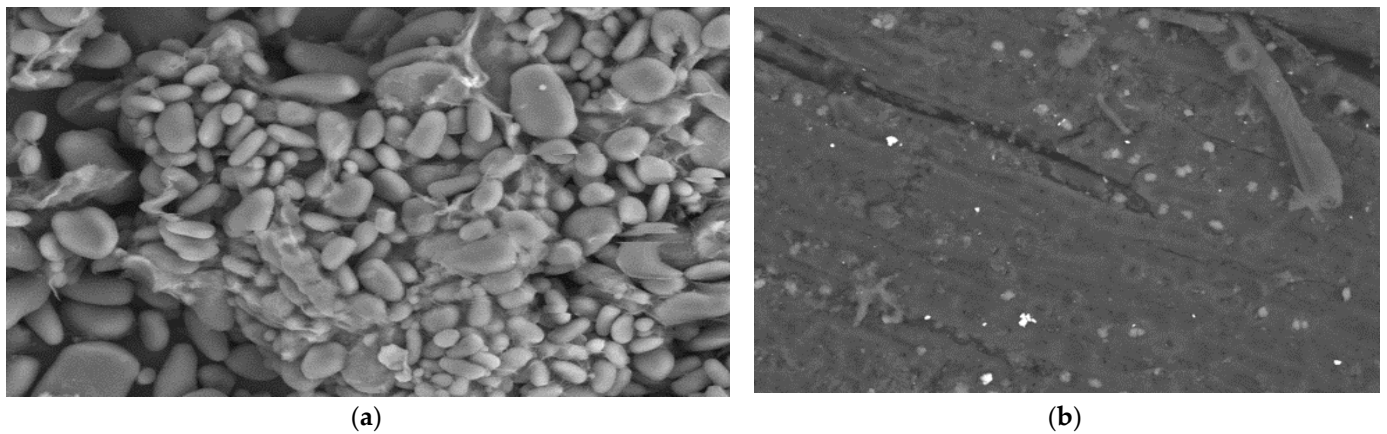


Figure 1. SEM micrographs of OPB (a) before and (b) after Cr (VI) adsorption with magnification of $\times 500$.

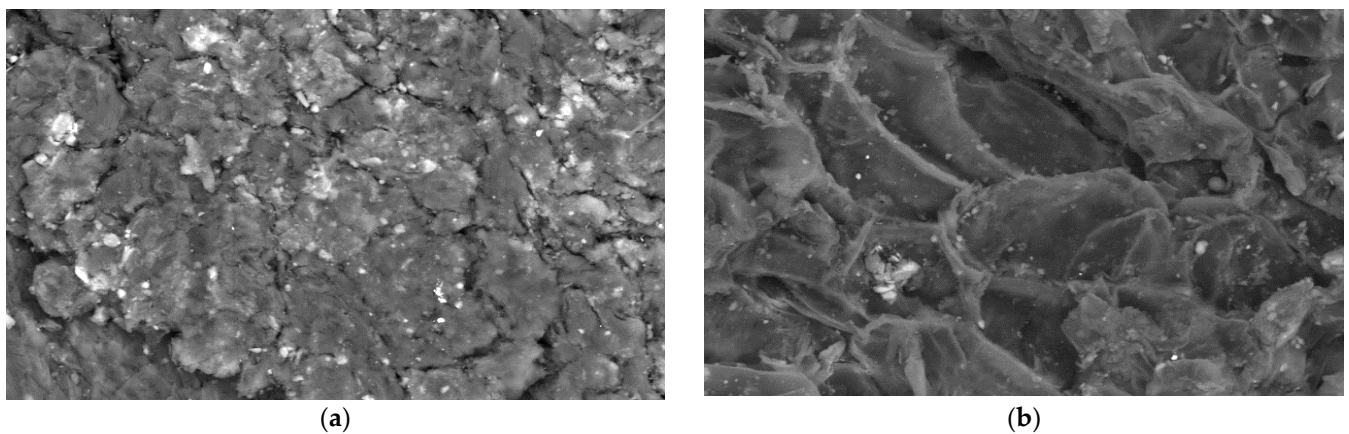


Figure 2. SEM micrographs of YP (a) before and (b) after Cr (VI) adsorption with magnification of $\times 500$.

Table 3. EDS composition analysis.

Element	OPB		OPB-Cr (VI)		YP		YP-Cr (VI)	
	Weight %	Atomic %	Weight %	Atomic %	Weight %	Atomic %	Weight %	Atomic %
C	50.90	2.36	48.65	56.49	47.40	57.07	54.50	63.25
O	44.60	2.22	48.82	42.56	43.20	39.05	39.67	34.56
Al					0.75	0.40	0.82	0.42
Si	3.87	0.20	1.12	0.56	2.16	1.11	1.21	0.60
P					0.66	0.31		
S					0.17	0.08		
K			0.20	0.07	4.46	1.65	0.44	0.16
Ca	0.19	0.05	0.25	0.09	0.34	0.12	0.99	0.34
Fe					0.60	0.16		
Cu	0.45	0.1	0.49	0.11	0.27	0.06		
Cl							0.45	0.18
Cr			0.48	0.13			0.88	0.24
Totals	100.00		100.00		100.00		100.00	

From the FTIR analysis, we established which functional groups are present, and which could also be involved in the adsorption of the metal under study. Thus, in Figure 3, the spectrum of the biomaterials evaluated before and after the adsorption of Cr (VI) can

be observed. From these, the shifting of the bands and broadening of the peaks after the adsorption process in both materials are observed.

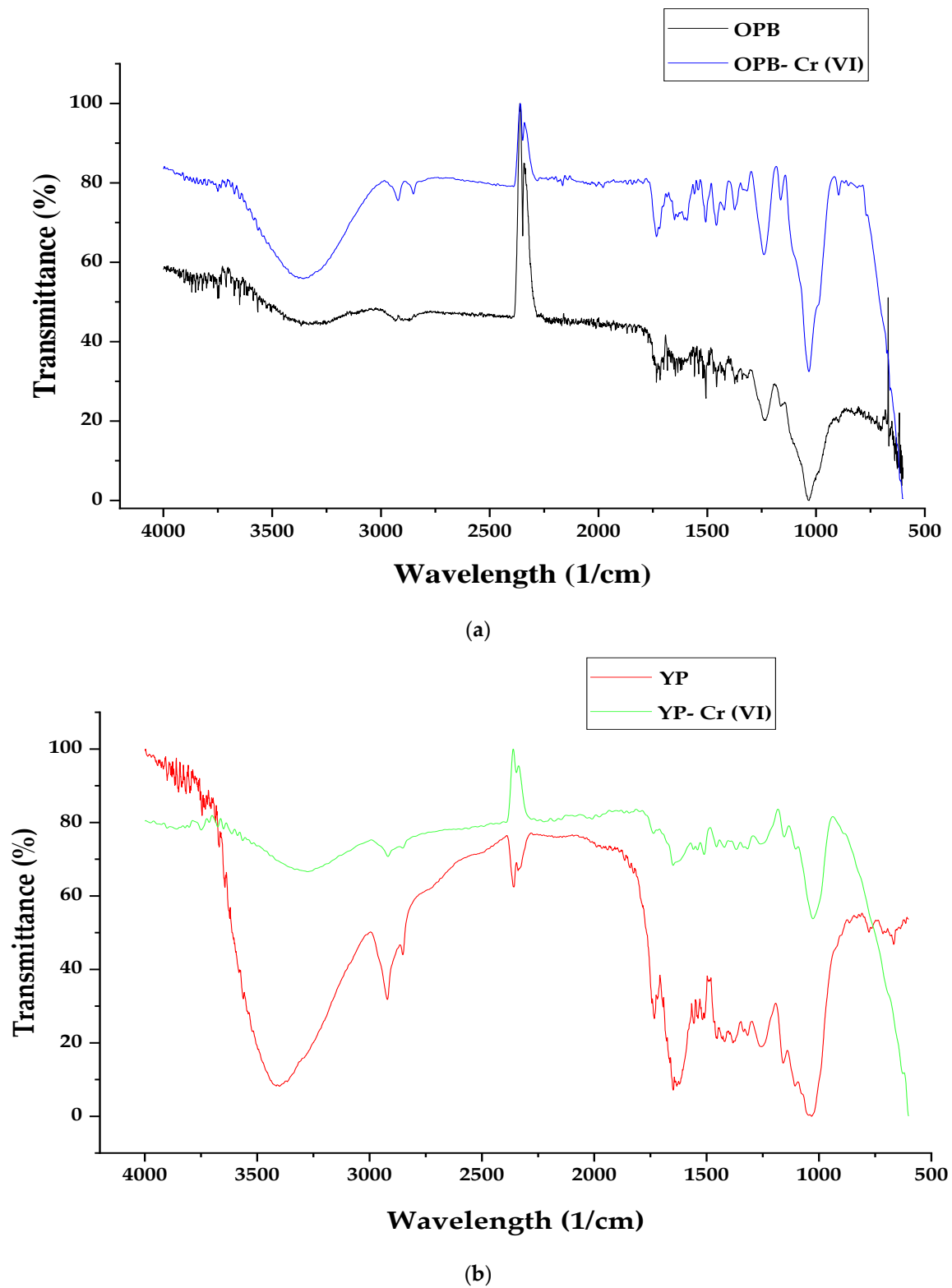


Figure 3. Normalized FTIR spectra for (a) OPB and (b) YP, before and after Cr (VI) adsorption.

The spectrum in Figure 3 initially shows a broad band at 3400 cm^{-1} that is attributed to the stretching vibrations of the OH bond, while the peaks at 2950 cm^{-1} and 1350 cm^{-1}

denote the C-H vibration [11]. The peak that appears at 1650 cm^{-1} corresponds to the intense signal characteristic of the stretching of the carbonyl group of carboxylic acids, as well as the one that appears at 1400 cm^{-1} related to the torsion of the carboxyl, and at 900 cm^{-1} the peak indicates the out-of-plane twisting of the carboxyl dimer [32]. The stretched band at 1150 cm^{-1} is related to the stretching of the COO⁻ anion, at 1080 cm^{-1} to the symmetric and asymmetric stretching of the C-O group of the ester vibration and at 1030 cm^{-1} to the functional group C-O-C [3]. The presence of hydroxyl groups, carbonyl groups, ethers and aromatic compounds is due to the high content of cellulose and lignin in the biomaterial; it is evidence of the lignocellulosic structure of the biomaterial under study, which contributes to the metal ion adsorption process [33].

3.2. Effect of the Temperature, Particle Size and Adsorbent Dose

From the hexavalent chromium adsorption tests using YP and OPB as the adsorbent, we evaluated the effect of temperature, particle size and amount of metal adsorbent by calculating the hexavalent chromium adsorption capacity using Equation (1). Table 4 lists the results of the experiments with their standard deviations (SD), to evaluate the adsorption capacity of Cr (VI) on OPB and YP.

Table 4. Experimental results for adsorption capacity of Cr (VI) onto OPB and YP, evaluating the effect of temperature, particle size and adsorbent dose.

Variable Conditions			Adsorption Capacity (mg/g)	
Temperature (°C)	Particle Size (mm)	Adsorbent Dose (g)	OPB	YP
40.0	0.355	0.15	38.36 ± 0.02	66.67 ± 0.07
70.0	1.0	0.15	15.82 ± 0.03	66.67 ± 0.04
40.0	1.0	0.5	18.02 ± 0.007	19.99 ± 0.04
55.0	0.5	0.62	14.89 ± 0.01	15.96 ± 0.01
55.0	0.14	0.325	7.15 ± 0.07	30.769 ± 0.08
80.0	0.5	0.325	30.77 ± 0.01	30.77 ± 0.01
55.0	1.22	0.325	30.77 ± 0.09	30.77 ± 0.05
29.8	0.5	0.325	25.22 ± 0.06	30.77 ± 0.07
55.0	0.5	0.03	325.88 ± 0.008	159.77 ± 0.001
70.0	0.355	0.15	66.66 ± 0.02	66.67 ± 0.04
40.0	1.0	0.15	34.21 ± 0.02	64.36 ± 0.08
55.0	0.5	0.325	29.48 ± 0.005	29.49 ± 0.006
40.0	0.355	0.5	19.99 ± 0.009	19.99 ± 0.04
70.0	1.0	0.5	4.69 ± 0.0005	19.99 ± 0.03
70.0	0.355	0.5	19.99 ± 0.03	19.99 ± 0.02
55.0	0.5	0.325	29.47 ± 0.002	29.49 ± 0.004

From the results presented in Table 4, we found that at 0.03 g of biomaterial, 0.5 mm of main particle size and 55 °C, the best adsorption was achieved for both biomaterials, reaching 159.77 mg/g when using YP and 325.88 mg/g with OPB. There is evidence of a decrease in adsorption capacity as the amount of biomaterial increases, which is due to the diversity of the biomasses evaluated, so there are a large number of active adsorption sites available due to the presence of the hydroxyl, carbonyl, amine and hydrocarbon groups present in the structure of lignin, hemicellulose, cellulose and pectin [22]. Due to this presence of active adsorption centers, it would appear that the greater the amount of adsorbent, the greater part of these would remain free after the process, thus decreasing the adsorption capacity [34].

The effect of temperature can be explained due to the stimulation of the active adsorption centers with the increase in temperature, as well as the increase in the intra-particle diffusion speed from the solution to the adsorbent, assuming that the diffusion is an endothermic process at the initial temperatures evaluated [35]. It is possible that at higher temperatures (70 and 80 °C) the interaction forces between adsorbate and adsor-

bent weaken [36]. An increase in temperature would favor the desorption of the sorbate molecules on the structure of the sorbent, since by gaining more energy than the bonds formed between the compound support, the forces of interaction are reduced and cause the release, which is what is not known [4].

In addition, it is evident that the adsorption capacity increases with particle size in the range 0.14 mm to 0.5 mm, and then decreases from 1.0 mm to 1.2 mm. This is explained by the influence of particle size on the surface contact area of the adsorbents, which increases when the particle size is smaller, and in turn, favors the rate of diffusion increased by increasing temperature [36]. However, a very small size would resist diffusive surface phenomena and subsequent mass transfer through the pores [37]. Considering that a smaller particle size increases the contact area between the adsorbent material and the ion, it would be expected that at 0.14 mm the best performance of YP and OPB can be obtained; however, this does not happen. This can be explained because Cr (VI) has an atomic radius of 1.27 Å and an ionic radius of 0.69 Å, which are smaller than the size of the pores of both adsorbents (23.04 nm for YP and 16.41 nm for YP). It has been shown that, as long as the radius of the particles is higher than the penetration depth of the diffusion, the adsorption capacity will increase, since, if the penetration of the contaminant is not sufficient, it would not increase the adsorption capacity [38]. Table 5 shows the results obtained from the analysis of variance (ANOVA), performed with the Statgraphics Centurión XVI.I software for the adsorption capacity of Cr (VI) on OPB and YP.

Table 5. Variance analysis for Cr (VI) adsorption capacity onto OPB and YP.

Factor	OPB			YP		
	Sum of Squares	F-Ratio	<i>p</i> -Value	Sum of Squares	F-Ratio	<i>p</i> -Value
A: Temperature	2.58	0.00	0.98	0.39	0.00	0.9697
B: Particle size	77.59	0.02	0.91	0.39	0.00	0.9697
C: Adsorbent dose	27,727.1	5.55	0.06	13301.7	53.51	0.0003
AA	1261.07	0.25	0.63	18.41	0.07	0.7946
AB	450.20	0.09	0.77	0.66	0.00	0.9604
AC	67.49	0.01	0.91	0.66	0.00	0.9604
BB	2046.08	0.41	0.55	18.41	0.07	0.7946
BC	177.76	0.04	0.86	0.66	0.00	0.9604
CC	13,858.1	2.77	0.15	3266.42	13.14	0.0110
Total error	29,980.2			1491.49		
Total (corr.)	87,589.2			19569.7		

From the values presented in Table 5, it was established that only for the adsorption of Cr (VI) when using YP does the amount of adsorbent (C) and its interaction CC have a significantly negative effect on the adsorption process. This is explained by the fact that the higher the amount of adsorbent, although there is higher removal efficiency, the material requirement increases to remove the same amount of metal ions. In the same way, when using a higher dose of material, there would be empty adsorption sites, thus reducing the retention capacity of the metal ions per available adsorbent mass [39]. It can be said that the temperature and the particle size do not have a significant influential effect on the adsorption capacity.

3.3. Adsorption Isotherm

The effect of the initial concentration on the adsorption capacity of Cr (VI) was evaluated by varying the concentration of the contaminant in intervals of 25 mg/L to 150 mg/L at pH 2 per 24 h, in order to understand the driving forces involved in the removal [40].

Figure 4 shows the non-linear fitting of experimental data to Langmuir, Freundlich, and Dubinin–Radushkevich models; the fitting parameters are summarized in Table 6, for the non-linearized and linearized forms of the models.

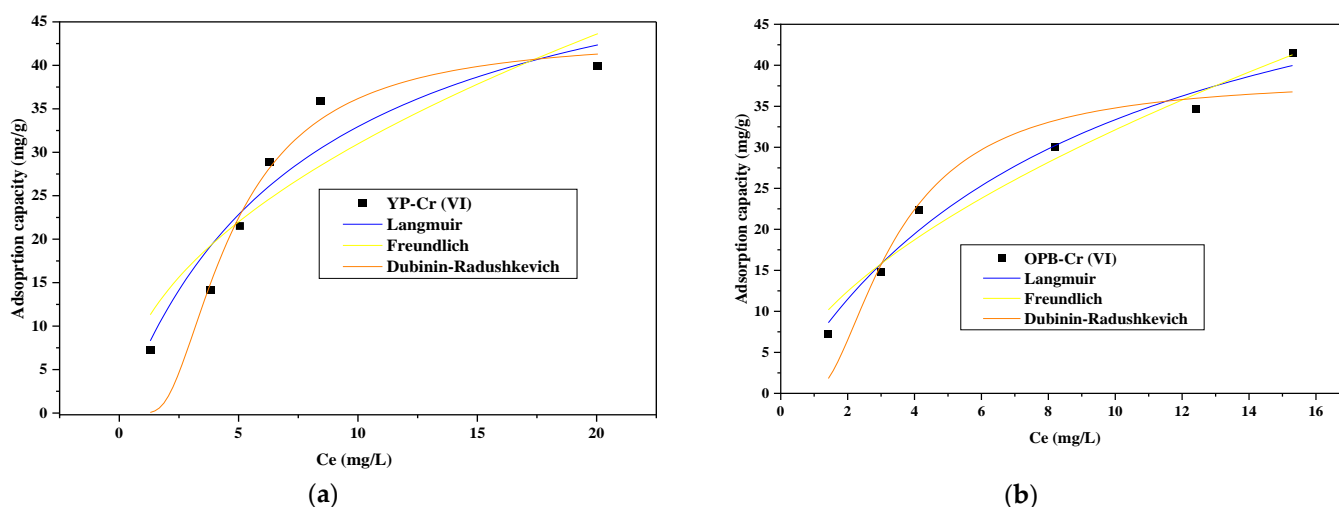


Figure 4. Modeling of hexavalent chromium adsorption isotherms over (a) YP and (b) OPB; at pH = 2, 200 rpm, 0.03 g of adsorbent dose and 55 °C.

Table 6. Adjustment parameters of hexavalent chromium adsorption isotherms on YP and OPB.

Model	Parameters	Non-Linear		Linear	
		YP	OPB	YP	OPB
Langmuir	q_{max} (mg/g)	59.16	63.83	60.60	68.49
	K_L	0.13	0.11	0.11	0.09
	R^2	0.89	0.98	0.89	0.94
Freundlich	K_f	9.94	8.27	6.74	6.65
	$1/n$	0.49	0.59	1.48	1.44
	n	2.03	1.69	0.68	0.69
	R^2	0.90	0.96	0.90	0.95
Dubinin–Radushkevich	q (mg/g)	43.28	38.39	38.95	32.9
	k_{DR}	2.65×10^{-6}	1.45×10^{-6}	6.86×10^{-6}	1.05×10^{-5}
	E	434.29	587.04	269.95	218.11
	R^2	0.91	0.90	0.85	0.90

The results reveal that Dubinin–Radushkevich’s model describes the equilibrium of hexavalent chromium adsorption on OPB, while Langmuir’s and Freundlich’s models adjust the isotherm of ion adsorption in the study on OPB, because it is established that the physical and chemical adsorption phenomena control the adsorption process; thus, the retention of the contaminant occurs inside and in the internal pores of the adsorbent [41]. Dubinin–Radushkevich’s model adjusts the isotherm on YP, with an average energy of adsorption of the ions per sorbate (E) of 434.29 kJ/mol, which is much higher than 8 kJ/mol, indicating that the process is mostly controlled by chemical adsorption with strong interactions between the active sites and the hexavalent chromium [42]. Dubinin–Radushkevich’s model presents a good fit for the equilibrium of chromium adsorption using the two adsorbents evaluated because the calculated maximum adsorption capacity (q_{DR}) values are the closest to the experimental ones, with $R^2 \geq 0.9$ in both cases. This means that the adsorbents under study present a heterogeneous structure, which is required for a good fitting by the Dubinin–Radushkevich isotherm [43]. Similar R^2 values to those obtained in the present study when the Dubinin–Radushkevich model was evaluated for removing Cr (VI) were found for *Pleurotus mutilus* ($R^2 = 0.93$) [44], *Sterculia villosa* (R^2 values between

0.81 and 0.96) [43], activated carbon from *Ziziphus jujuba* (R^2 between 0.98 and 0.99) [18] and rice husk ($R^2 = 0.93$) [45].

Table 7 presents a comparison of results from previous studies when using lignocellulosic-based adsorbents for removing Cr (VI). It is observed that in all cases the adsorption process was evaluated at acid pH. In addition, a better performance was obtained for the OPB and YP; this might be due to the contact time between the adsorbate and adsorbent.

Table 7. Maximum adsorption capacity comparison of different adsorbent materials.

Adsorbent	Conditions	q_{max} (mg/g)	Reference
Oil palm fuel ash	pH = 2, 200 rpm, 80 g/L of adsorbent	0.462	[5]
Banana peel dust	pH = 1, 0.4 g of adsorbent dose, 300 rpm, 50 °C	26.46	[12]
Modified lychee peel	50 °C, pH = 2, 130 rpm, 0.08 g of adsorbent and 20 mL of solution	9.76	[17]
Foxtail millet shell	4 g/L of adsorbent dose, 0.25–0.35 mm of particle size, 30 mL of solution, 120 min, 350 rpm, and 25 °C	11.70	[21]
Oil palm bagasse	pH = 2, 200 rpm, 55 °C, 24 h	63.83	This work
Yam peel		59.16	

3.4. Kinetics of Adsorption

The kinetic study is important to determine the behavior of the adsorption process over time. Figure 5 shows the non-linear fit of the kinetic curves obtained for the removal of Cr (VI) on OPB and YP, and it is observed that the equilibrium times were 200 and 400 min for each adsorbent evaluated.

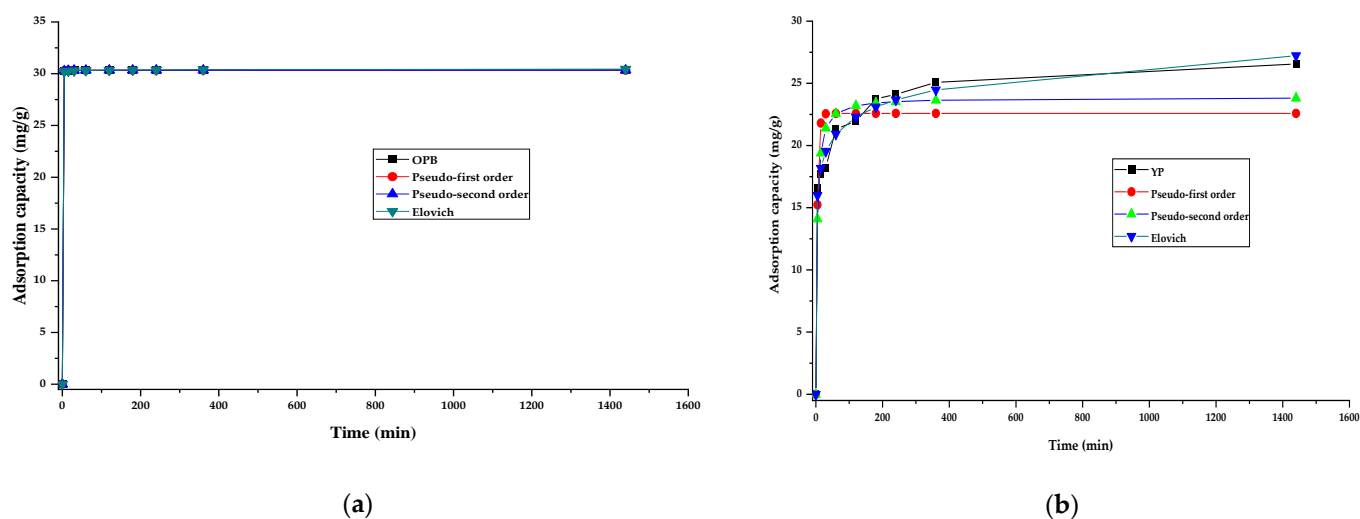


Figure 5. Non-linear fit to kinetic models of Cr (VI) adsorption on (a) OPB and (b) YP; at pH = 2, 200 rpm, 0.03 g of sweet adsorbent, 100 mg/L of initial concentration and 55 °C.

For both biomaterials, it is highlighted that about 70% of the equilibrium concentration was reached 120 min after the start of the test, showing that the available sites in the adsorbent probably begin to saturate and therefore the capacity does not change significantly at higher times [45]. In order to study the adsorption mechanisms involved during the Cr (VI) removal process, pseudo-first-order, pseudo-second-order and Elovich linearized kinetic models were used, in their non-linearized forms. The parameters of these models were adjusted by linear regression and the results are shown in Table 8.

Table 8. Adjustment parameters of kinetic models.

Model	Parameters	OPB	YP
Pseudo-first-order	q_e	30.33	22.58
	k_1	1.334	0.23
	SS	0.009	64.93
	R^2	0.9999	0.9359
Pseudo-second-order	q_e	2,499,562.65	3925.03
	k_2	30.34	23.87
	SS	0.006	32.29
	R^2	0.9999	0.9961
Elovich	β	23.27	0.50
	α	1.25×10^{30}	1247.80
	SS	0.02	4.03
	R^2	0.9999	0.9867

For the YP-Cr (VI) system, it is evidenced that the three evaluated models present a good fit of the experimental data with $R^2 > 0.99$ in all cases, indicating that the removal process occurs through physis and chemisorption, due to the heterogeneity of the active centers of the YP [18]. However, the pseudo-second-order model is the one that describes the experimental data of removal of the metal under study on OPB, which indicates that the adsorption occurs by chemical reaction between the functional groups of the biomaterial and the metal ions [46]. From the values of the reaction rate constants of the pseudo-first- (k_1) and pseudo-second-order (k_2) models, it can be said that the initial sorption rate on YP is lower than for OPB, the latter presenting a greater adsorption capacity, which could be due to the fibrous nature of the OPB, as well as its superior surface area [5].

Previous results have been reported regarding the adsorption capacity of different materials such as 13.48 mg/g when using coffee pulp [3], 10.31 mg/g for lime peel [4] and 28 mg/g while using kenaf fiber [9], compared to 31.34 and 23.87 mg/g for OPB and YP, respectively, found in the present study. We note that these results are superior to the others mentioned for adsorbents prepared from residual crude lignocellulosic biomass. From the results obtained when using activated carbon from melon peel in the removal of Cr (VI), it was found that the process can be described by the Elovich equation, so that the limiting step in the adsorption of the metal ions may be the chemical interaction between metal ions and functional groups on the surface of the adsorbent [1].

3.5. Thermodynamic Adsorption Parameters

By calculating the thermodynamic parameters, it is possible to establish the feasibility, the adsorption mechanism, the energetic character of the process (endothermic or exothermic) and the spontaneity of the adsorption; this is done by determining the entropy (ΔS°), enthalpy (ΔH°) and the change in Gibbs free energy (ΔG°), respectively. In Figure 6, we present the van't Hoff equation by graphing to 81 °C, considering the conditions established in the design of experiments; a graph was plotted of $\ln(K_c)$ vs. $1/T$.

The thermodynamic parameters of hexavalent chromium adsorption on OPB and YP are summarized in Table 9. From the positive value of ΔH° when using YP it is established that the processes of chromium removal are endothermic; consequently, energy must be supplied to the system to promote the diffusive phenomena in the solution and inside the pores of the adsorbent [32]. For OPB the process is exothermic and the limiting step is chemical adsorption [47]. The negative value of ΔS° shows that on the surface there was a good bond between the metal and the biomass, thus obtaining a low possibility of reversibility; there was also the probability of some structural changes due to the formation of bonds with functional groups at the interface [42].

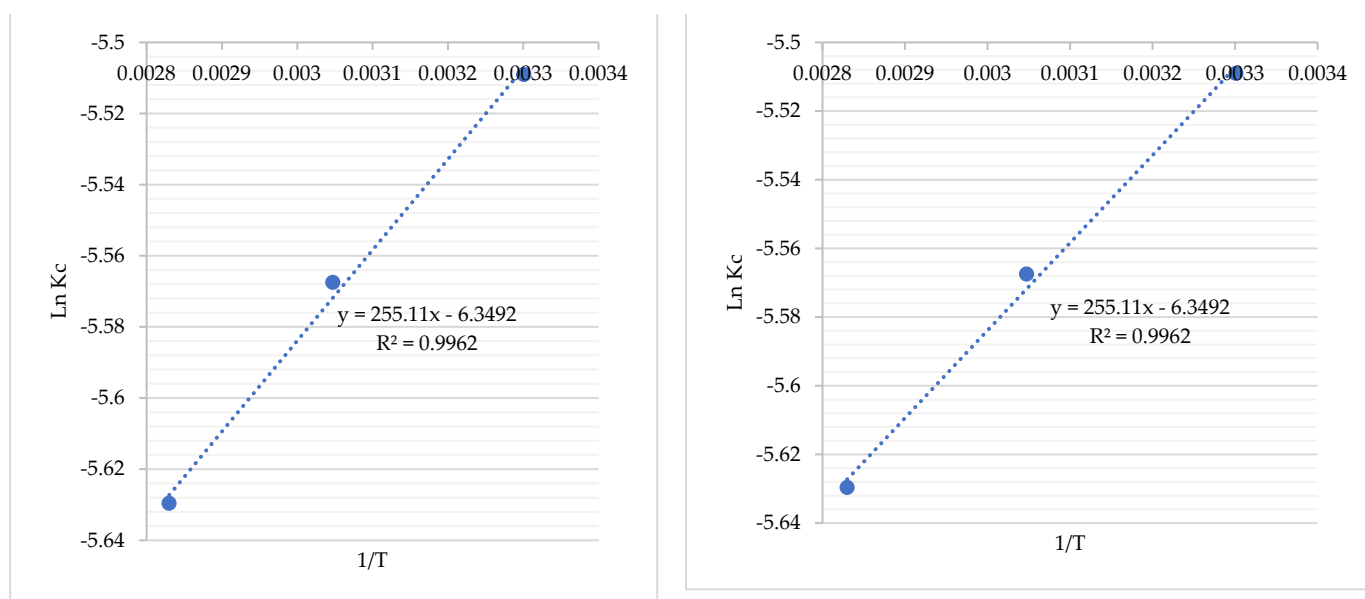


Figure 6. $\ln K_c$ vs. $1/T$ plot for thermodynamic parameters calculation.

Table 9. Thermodynamic parameters for the adsorption of hexavalent chromium at pH 2, 200 rpm, 0.325 g of adsorbent dose, 0.5 mm of particle size and 100 mg/L of initial concentration.

Biomass	T (K)	ΔG^0 (kJ/mol)	ΔH^0 (kJ/mol)	ΔS^0 (kJ/mol \times K)
OPB	302.95	−13.1779	−7.9993	−0.0698
	328.15	−14.9243		
	353.15	−16.6701		
YP	302.95	14.1406	4.3693	−0.029
	328.15	15.3020		
	353.15	16.4635		

4. Conclusions

SEM-EDS and FTIR analysis of OPB and YP showed that they present a porous surface typical of lignocellulosic materials, with the presence of hydroxyl, amine and carboxyl functional groups. From the adsorption experiments, the highest adsorption capacity was obtained at 0.03 g of adsorbent, 55 °C and 0.5 mm, reporting 325.88 and 159 mg/g using OPB and YP, respectively. We obtained a maximum adsorption capacity of 63.83 mg/g with OPB and 59.16 mg/g using YP, according to the Langmuir model. The equilibrium of adsorption on OPB was described by the Langmuir and Freundlich models, while YP was described by the Dubinin–Radushkevich model, whose parameters of fitting suggest that adsorption is given by ion exchange between the active centers and the metal ions. A kinetic study demonstrated that equilibrium time was 200 min for both materials; kinetic data were described by pseudo-second-order and Elovich models; thus, the mechanism of Cr (VI) adsorption onto the evaluated materials was dominated by a chemical reaction. The thermodynamic parameters determined that the removal for YP is endothermic, irreversible and non-spontaneous, while for OPB it is exothermic, spontaneous at low temperatures and irreversible. The rapid removal rate and high adsorption capacities obtained show that the adsorbents evaluated are effective in the removal of hexavalent chromium present in aqueous solution.

Author Contributions: C.T.-T., Á.G.-D. and A.V.-O. conceived and designed the paper, and wrote the Introduction and Materials and Methods. C.T.-T. and A.V.-O. wrote the Results and prepared figures and tables. Discussions and Conclusions were the collective work of all authors. The writing—review and editing was performed by Á.G.-D. All authors have read and agreed to the published version of the manuscript.

Funding: This investigation did not have external funding.

Data Availability Statement: The data that support the findings of this study are available on request from the corresponding author.

Acknowledgments: The authors thank the Universidad de Cartagena for the support to develop this research, as well as laboratories, software and time of the research team.

Conflicts of Interest: The authors declare no conflict of interest.

References

1. Manjuladevi, M.; Anitha, R.; Manonmani, S. Kinetic study on adsorption of Cr (VI), Ni (II), Cd (II) and Pb (II) ions from aqueous solutions using activated carbon prepared from Cucumis melo peel. *Appl. Water Sci.* **2018**, *8*, 36. [[CrossRef](#)]
2. Feizi, M.; Jalali, M. Removal of heavy metals from aqueous solutions using sunflower, potato, canola and walnut shell residues. *J. Taiwan Inst. Chem. Eng.* **2015**, *54*, 125–136. [[CrossRef](#)]
3. Gómez-Aguilar, D.L.; Rodríguez-Miranda, J.P.; Esteban-Muñoz, J.A.; Betancur, J.F. Coffee Pulp: A Sustainable Alternative Removal of Cr (VI) in Wastewaters. *Processes* **2019**, *7*, 403. [[CrossRef](#)]
4. Premkumar, P.; Sudha, R. Comparative studies on the removal of chromium (VI) from aqueous solutions using raw and modified Citrus Limetioides peel. *Indian J. Chem. Technol.* **2018**, *25*, 255–265.
5. Nordin, N.; Asmadi, N.A.A.; Manikam, M.K.; Halim, A.A.; Hanafiah, M.M.; Hurairah, S.N. Removal of Hexavalent Chromium from Aqueous Solution by Adsorption on Palm Oil Fuel Ash (POFA). *J. Geosci. Environ. Prot.* **2020**, *8*, 112–127. [[CrossRef](#)]
6. Bhanvase, B.A.; Ugwekar, R.P.; Mankar, R.B. (Eds.) *Novel Water Treatment and Separation Methods*; Apple Academic Press: Toronto, NJ, Canada, 2017.
7. Tran, H.N.; Nguyen, D.T.; Le, G.T.; Tomul, F.; Lima, E.C.; Woo, S.H.; Sarmah, A.K.; Nguyen, H.Q.; Nguyen, P.T.; Nguyen, D.D.; et al. Adsorption mechanism of hexavalent chromium onto layered double hydroxides-based adsorbents: A systematic in-depth review. *J. Hazard. Mater.* **2019**, *373*, 258–270. [[CrossRef](#)] [[PubMed](#)]
8. Núñez-Zarur, J.; Tejada-Tovar, C.; Villabona-Ortíz, A.; Acevedo, D.; Tejada-Tovar, R. Thermodynamics, Kinetics and Equilibrium Adsorption of Cr (VI) and Hg (II) in Aqueous Solution on corn cob (*Zea mays*). *Int. J. ChemTech Res.* **2018**, *11*, 265–280.
9. Omidvar-Borna, M.; Pirsaeheb, M.; Vosoughi-Niri, M.; Khosravi-Mashizie, R.; Kakavandi, B.; Zare, M.R.; Asadi, A. Batch and column studies for the adsorption of chromium(VI) on low-cost Hibiscus Cannabinus kenaf, a green adsorbent. *J. Taiwan Inst. Chem. Eng.* **2016**, *68*, 80–89. [[CrossRef](#)]
10. Corral-Escárcega, M.C.; Ruiz-Gutiérrez, M.G.; Quintero-Ramos, A.; Meléndez-Pizarro, C.O.; Lardizabal-Gutiérrez, D.; Campos-Venegas, K. Use of biomass-derived from pecan nut husks (*Carya illinoensis*) for chromium removal from aqueous solutions. column modeling and adsorption kinetics studies. *Rev. Mex. Ing. Quim.* **2017**, *16*, 939–953.
11. Ben Khalifa, E.; Rzig, B.; Chakroun, R.; Nouagui, H.; Hamrouni, B. Application of response surface methodology for chromium removal by adsorption on low-cost biosorbent. *Chemom. Intell. Lab. Syst.* **2019**, *189*, 18–26. [[CrossRef](#)]
12. Mondal, N.K.; Samanta, A.; Chakraborty, S.; Shaikh, W.A. Enhanced chromium (VI) removal using banana peel dust: Isotherms, kinetics and thermodynamics study. *Sustain. Water Resour. Manag.* **2017**, *4*, 489–497. [[CrossRef](#)]
13. Mahmood-Ul-Hassan, M.; Yasin, M.; Youstra, M.; Ahmad, R.; Sarwar, S. Kinetics, isotherms, and thermodynamic studies of lead, chromium, and cadmium bio-adsorption from aqueous solution onto Picea smithiana sawdust. *Environ. Sci. Pollut. Res.* **2018**, *25*, 12570–12578. [[CrossRef](#)] [[PubMed](#)]
14. Torres Pérez, C.I.; Quintero Lopez, L.A. Analysis of African palm solid waste, as an alternative to use renewable energy in the department of Cesar. *Ing. USBMed* **2019**, *10*, 8–18. [[CrossRef](#)]
15. Souza, P.R.; Dotto, G.L.; Salau, N.P.G. Artificial neural network (ANN) and adaptive neuro-fuzzy interference system (ANFIS) modelling for nickel adsorption onto agro-wastes and commercial activated carbon. *J. Environ. Chem. Eng.* **2018**, *6*, 7152–7160. [[CrossRef](#)]
16. Astudillo, P.; Isabel, C.; Barrero, R.; Carlos, A.; Puella, B.; Luis, M. Diagnostic of the main agricultural residues produced in the Bolivar region. *Sci. Agroaliment.* **2015**, *2*, 39–50.
17. Yi, Y.; Lv, J.; Liu, Y.; Wu, G. Synthesis and application of modified Litchi peel for removal of hexavalent chromium from aqueous solutions. *J. Mol. Liq.* **2017**, *225*, 28–33. [[CrossRef](#)]
18. Labied, R.; Benturki, O.; Eddine Hamitouche, A.Y.; Donnot, A. Adsorption of hexavalent chromium by activated carbon obtained from a waste lignocellulosic material (*Ziziphus jujuba cores*): Kinetic, equilibrium, and thermodynamic study. *Adsorpt. Sci. Technol.* **2018**, *36*, 1066–1099. [[CrossRef](#)]
19. Heffron, J.; Marhefke, M.; Mayer, B.K. Removal of trace metal contaminants from potable water by electrocoagulation. *Sci. Rep.* **2016**, *6*, 28478. [[CrossRef](#)]
20. Mädler, S.; Sun, F.; Tat, C.; Sudakova, N.; Drouin, P.; Tooley, R.J.; Reiner, E.J.; Switzer, T.A.; Dyer, R.; Kingston, H.M.S.; et al. Trace-Level Analysis of Hexavalent Chromium in Lake Sediment Samples Using Ion Chromatography Tandem Mass Spectrometry. *J. Environ. Prot.* **2016**, *7*, 422–434. [[CrossRef](#)]
21. Peng, S.H.; Wang, R.; Yang, L.Z.; He, L.; He, X.; Liu, X. Biosorption of copper, zinc, cadmium and chromium ions from aqueous solution by natural foxtail millet shell. *Ecotoxicol. Environ. Saf.* **2018**, *165*, 61–69. [[CrossRef](#)]

22. Cherdchoo, W.; Nithettham, S.; Charoenpanich, J. Removal of Cr (VI) from synthetic wastewater by adsorption onto coffee ground and mixed waste tea. *Chemosphere* **2019**, *221*, 758–767. [[CrossRef](#)] [[PubMed](#)]
23. Ayawei, N.; Ebelegi, A.N.; Wankasi, D. Modelling and Interpretation of Adsorption Isotherms. *J. Chem.* **2017**, *2017*. [[CrossRef](#)]
24. Rasmey, A.-H.M.; Aboseidah, A.A.; Youssef, A.K. Application of Langmuir and Freundlich Isotherm Models on Biosorption of Pb²⁺ by Freeze-dried Biomass of *Pseudomonas aeruginosa*. *Egypt. J. Microbiol.* **2018**, *53*, 37–48. [[CrossRef](#)]
25. Akpomie, K.G.; Eluke, L.O.; Ajiwe, V.I.E.; Alisa, C.O. Attenuation kinetics and desorption performance of artocarpus altilis seed husk for Co (II), Pb (II) And Zn (II) Ions. *Iran. J. Chem. Chem. Eng.* **2018**, *37*, 171–186.
26. Blanes, P.S.; Bordoní, M.E.; González, J.C.; García, S.I.; Atria, A.M.; Sala, L.F.; Bellú, S.E. Application of soy hull biomass in removal of Cr (VI) from contaminated waters. Kinetic, thermodynamic and continuous sorption studies. *J. Environ. Chem. Eng.* **2016**, *4*, 516–526. [[CrossRef](#)]
27. Tran, H.N.; You, S.J.; Chao, H.P. Thermodynamic parameters of cadmium adsorption onto orange peel calculated from various methods: A comparison study. *J. Environ. Chem. Eng.* **2016**, *4*, 2671–2682. [[CrossRef](#)]
28. Manirethan, V.; Gupta, N.; Balakrishnan, R.M.; Raval, K. Batch and continuous studies on the removal of heavy metals from aqueous solution using biosynthesised melanin-coated PVDF membranes. *Environ. Sci. Pollut. Res.* **2019**, *27*, 1–15. [[CrossRef](#)]
29. Asuquo, E.D.; Martin, A.D. Sorption of cadmium (II) ion from aqueous solution onto sweet potato (*Ipomoea batatas* L.) peel adsorbent: Characterisation, kinetic and isotherm studies. *J. Environ. Chem. Eng.* **2016**, *4*, 4207–4228. [[CrossRef](#)]
30. Asuquo, E.; Martin, A.; Nzerem, P.; Siperstein, F.; Fan, X. Adsorption of Cd(II) and Pb(II) ions from aqueous solutions using mesoporous activated carbon adsorbent: Equilibrium, kinetics and characterisation studies. *J. Environ. Chem. Eng.* **2017**, *5*, 679–698. [[CrossRef](#)]
31. Pradhan, P.; Arora, A.; Mahajani, S.M. Pilot scale evaluation of fuel pellets production from garden waste biomass. *Energy Sustain. Dev.* **2018**, *43*, 1–14. [[CrossRef](#)]
32. Afroze, S.; Sen, T.K. A review on heavy metal ions and dye adsorption from water by agricultural solid waste adsorbents. *Water Air Soil Pollut.* **2018**, *229*, 225. [[CrossRef](#)]
33. Vu, X.H.; Nguyen, L.H.; Van, H.T.; Nguyen, D.V.; Nguyen, T.H.; Nguyen, Q.T.; Ha, L.T. Adsorption of Chromium (VI) onto Freshwater Snail Shell-Derived Biosorbent from Aqueous Solutions: Equilibrium, Kinetics, and Thermodynamics. *J. Chem.* **2019**, *2019*, 1–11. [[CrossRef](#)]
34. Chakraborty, P.; Show, S.; Ur Rahman, W.; Halder, G. Linearity and non-linearity analysis of isotherms and kinetics for ibuprofen removal using superheated steam and acid modified biochar. *Process Saf. Environ. Prot.* **2019**, *126*, 193–204. [[CrossRef](#)]
35. Wu, Y.; Fan, Y.; Zhang, M.; Ming, Z.; Yang, S.; Arkin, A. Functionalized agricultural biomass as a low-cost adsorbent: Utilization of rice straw incorporated with amine groups for the adsorption of Cr (VI) and Ni (II) from single and binary systems. *Biochem. Eng. J.* **2016**, *105*, 27–35. [[CrossRef](#)]
36. Haroon, H.; Ashfaq, T.; Gardazi, S.M.H.; Sherazi, T.A.; Ali, M.; Rashid, N.; Bilal, M. Equilibrium kinetic and thermodynamic studies of Cr (VI) adsorption onto a novel adsorbent of *Eucalyptus camaldulensis* waste: Batch and column reactors. *Korean J. Chem. Eng.* **2016**, *33*, 2898–2907. [[CrossRef](#)]
37. Cai, J.; He, Y.; Yu, X.; Banks, S.W.; Yang, Y.; Zhang, X.; Yu, Y.; Liu, R.; Bridgwater, A.V. Review of physicochemical properties and analytical characterization of lignocellulosic biomass. *Renew. Sustain. Energy Rev.* **2017**, *76*, 309–322. [[CrossRef](#)]
38. Pan, L.; Nishimura, Y.; Takaesu, H.; Matsui, Y.; Matsushita, T.; Shirasaki, N. Effects of decreasing activated carbon particle diameter from 30 µm to 140 nm on equilibrium adsorption capacity. *Water Res.* **2017**, *124*, 425–434. [[CrossRef](#)] [[PubMed](#)]
39. Ibisí, N.; Asoluka, C. Use of agro-waste (*Musa paradisiaca* peels) as a sustainable biosorbent for toxic metal ions removal from contaminated water. *Chem. Int.* **2018**, *4*, 52–59.
40. Villabona-Ortíz, A.; Tejada-Tovar, C.; Ortega-Toro, R. Modelling of the adsorption kinetics of Chromium (VI) using waste biomaterials. *Rev. Mex. Ing. Química* **2020**, *19*, 401–408. [[CrossRef](#)]
41. Da'Na, E.; Awad, A. Regeneration of spent activated carbon obtained from home filtration system and applying it for heavy metals adsorption. *J. Environ. Chem. Eng.* **2017**, *5*, 3091–3099. [[CrossRef](#)]
42. Ajmani, A.; Shahnaz, T.; Subbiah, S.; Narayanasamy, S. Hexavalent chromium adsorption on virgin, biochar, and chemically modified carbons prepared from *Phanera vahlii* fruit biomass: Equilibrium, kinetics, and thermodynamics approach. *Environ. Sci. Pollut. Res.* **2019**, *26*, 32137–32150. [[CrossRef](#)] [[PubMed](#)]
43. Patra, C.; Mediseti, R.M.N.; Pakshirajan, K.; Narayanasamy, S. Assessment of raw, acid-modified and chelated biomass for sequestration of hexavalent chromium from aqueous solution using *Sterculia villosa* Roxb. shells. *Environ. Sci. Pollut. Res.* **2019**, *26*, 23625–23637. [[CrossRef](#)] [[PubMed](#)]
44. Alouache, A.; Selatnia, A.; Sayah, H.E.; Khodja, M.; Moussous, S.; Daoud, N. Biosorption of hexavalent chromium and Congo red dye onto *Pleurotus mutilus* biomass in aqueous solutions. *Int. J. Environ. Sci. Technol.* **2021**, 1–16. [[CrossRef](#)]
45. Khalil, U.; Shakoob, M.B.; Ali, S.; Ahmad, S.R.; Rizwan, M.; Alsahli, A.A.; Alyemeni, M.N. Selective removal of hexavalent chromium from wastewater by rice husk: Kinetic, isotherm and spectroscopic investigation. *Water* **2021**, *13*, 263. [[CrossRef](#)]
46. Alorabi, A.Q.; Alharthi, F.A.; Azizi, M.; Al-Zaqri, N.; El-Marghany, A.; Abdelshafeek, K.A. Removal of lead(II) from synthetic wastewater by *lavandula pubescens* decne biosorbent: Insight into composition–adsorption relationship. *Appl. Sci.* **2020**, *10*, 7450. [[CrossRef](#)]
47. Amro, A.N.; Abhary, M.K.; Shaikh, M.M.; Ali, S. Removal of lead and cadmium ions from aqueous solution by adsorption on a low-cost Phragmites biomass. *Processes* **2019**, *7*, 406. [[CrossRef](#)]